Aberrant TIMP-1 overexpression in tumor-associated fibroblasts drives tumor progression through CD63 in lung adenocarcinoma

Paula Duch [a], Natalia Díaz-Valdivia [a], Rafael Ikemori [a], Marta Gabasa [a,b], Evette S. Radisky [c], Marselina Arshakyan [a], Sabrina Gea-Sorlí [d,e], Anna Mateu-Bosch [d,e], Paloma Bragado [f,g], Josep Lluís Carrasco [h], Hidetoshi Mori [i], Josep Ramírez [b,j,k], Cristina Teixidó [b,d,j], Noemí Reguart [b,d], Cristina Fillat [d,e,l], Derek C. Radisky [c] and Jordi Alcaraz [a,b,m]

***a* - Unit of Biophysics and Bioengineering,,** *Department of Biomedicine, School of Medicine and Health Sciences, Universitat de Barcelona, Barcelona 08036, Spain*
***b* - Thoracic Oncology Unit,** *Hospital Clinic Barcelona, Barcelona 08036, Spain*
***c* - Department of Cancer Biology,** *Mayo Clinic, Jacksonville, FL 32224, United States*
***d* - Institut d'Investigacions Biomèdiques August Pi i Sunyer (IDIBAPS),** *Barcelona 08036, Spain*
***e* - Centro de Investigación Biomédica en Red de Enfermedades Raras (CIBERER),** *Madrid 08029, Spain*
***f* - Instituto de Investigaciones Sanitarias San Carlos (IdISSC),** *Madrid 28040, Spain*
***g* - Departamento de Bioquímica y Biología Molecular, Facultad de Farmacia,** *Universidad Complutense, Madrid 28040, Spain*
***h* - Unit of Biostatistics,,** *Department of Basic Clinical Practice, School of Medicine and Health Sciences, Universitat de Barcelona, Barcelona, Spain*
***i* - Center for Immunology and Infectious Diseases,** *University of California Davis, Davis, CA 95616, United States*
***j* - Pathology Service,** *Hospital Clínic de Barcelona, Barcelona 08036, Spain*
***k* - Centro de Investigación Biomédica en Red de Enfermedades Respiratorias (CIBERES), Instituto de Salud Carlos III,** *Madrid 28029, Spain*
***l* - Department of Medicine,** *School of Medicine and Health Sciences, Universitat de Barcelona, Barcelona, Spain*
***m* - Institute for Bioengineering of Catalonia (IBEC),** *The Barcelona Institute for Science and Technology (BIST), Barcelona 08028, Spain*

Corresponding author. ***jalcaraz@ub.edu.***
https://doi.org/10.1016/j.matbio.2022.06.009

Abstract

Tissue inhibitor of metalloproteinase-1 (TIMP-1) is an important regulator of extracellular matrix turnover that has been traditionally regarded as a potential tumor suppressor owing to its inhibitory effects of matrix metalloproteinases. Intriguingly, this interpretation has been challenged by the consistent observation that increased expression of TIMP-1 is associated with poor prognosis in virtually all cancer types including lung cancer, supporting a tumor-promoting function. However, how TIMP-1 is dysregulated within the tumor microenvironment and how it drives tumor progression in lung cancer is poorly understood. We analyzed the expression of TIMP-1 and its cell surface receptor CD63 in two major lung cancer subtypes: lung adenocarcinoma (ADC) and squamous cell carcinoma (SCC), and defined the tumor-promoting effects of their interaction. We found that TIMP-1 is aberrantly overexpressed in tumor-associated fibroblasts (TAFs) in ADC compared to SCC. Mechanistically, TIMP-1 overexpression was mediated by the selective hyperactivity of the pro-fibrotic TGF-β1/SMAD3 pathway in ADC-TAFs. Likewise, CD63 was upregulated in ADC compared to SCC cells. Genetic analyses revealed that TIMP-1 secreted by TGF-β1-activated ADC-TAFs is both necessary and sufficient to enhance growth and invasion of ADC cancer cells in culture, and that tumor cell expression of CD63 was required for these effects. Consistently, *in vivo* analyses revealed that ADC cells co-injected with fibroblasts with reduced SMAD3 or TIMP-1 expression into immunocompromised mice attenuated tumor aggressiveness compared to tumors bearing parental fibroblasts. We also found that high *TIMP1* and *CD63* mRNA levels combined define a stronger prognostic biomarker than *TIMP1* alone. Our results identify an excessive stromal TIMP-1 within the tumor microenvironment selectively in lung ADC, and

implicate it in a novel tumor-promoting TAF-carcinoma crosstalk, thereby pointing to TIMP-1/CD63 interaction as a novel therapeutic target in lung cancer.

Introduction

Lung cancer is the leading cause of cancer-related deaths worldwide, with a 5-year survival rate of ~19% [1]. Histologically, non-small cell lung cancer (NSCLC) is diagnosed in up to 85% of lung cancer patients, and is subdivided into adenocarcinoma (ADC; ~50%), squamous cell carcinoma (SCC; ~40%), and other less frequent subtypes [2]. Although both ADC and SCC are epithelial in origin, it is now clear that the fibrotic tumor microenvironment or desmoplastic stroma rich in tumor-associated fibroblasts (TAFs) is a critical contributor to tumor progression and resistance to therapies [3]. Lung TAFs are epigenetically reprogrammed and exhibit an activated/myofibroblast-like phenotype [4–6], which accounts for the excessive deposition of fibrillar collagens and other pro-fibrotic extracellular matrix (ECM) components within the tumor stroma [6,7]. Likewise, activated TAFs secrete ECM degrading proteases and other ECM remodeling factors to ultimately facilitate cancer cell proliferation, dissemination and angiogenesis [3,8]. Accordingly, there is growing therapeutic interest in identifying those TAF-dependent factors within the tumor microenvironment that drive tumor progression.

Tissue inhibitor of metalloproteinases-1 (TIMP-1) belongs to a family of four secreted proteins that are generally expressed in the tissue stroma [9]. TIMP-1 was initially considered as a potentially favorable cancer biomarker because it was first discovered as a natural inhibitor of matrix metalloproteinases (MMPs), which facilitate cancer dissemination through proteolytic degradation of the ECM; moreover, there is evidence that TIMP-1 can also have inhibitory effects on proliferation [10]. However, more recent studies have identified a strong association between TIMP-1 expression and poor outcome in NSCLC [11], and have reported that TIMP-1 is the only TIMP member that is both markedly overexpressed and associated with poor prognosis in lung cancer [9], thereby favoring a tumor-promoting function. Likewise, TIMP-1 is emerging as an important factor in orchestrating tumor progression in other cancer types [9], since both tissue and blood levels of TIMP-1 have been consistently associated with poor prognosis in virtually all human cancers [11,12], which granted its inclusion in a panel for early cancer detection [13]. In addition, there is growing evidence that TIMP-1 may promote cancer cell growth, invasion and even metastasis through cytokine-like functions [14–16].

The diverse and often opposing functions of TIMP-1 have been partially resolved by the identification of its structure in two functionally independent and physically distinct domains: the N-terminal domain that binds to and inhibits MMPs, and the C-terminal domain, which exhibits cytokine-like functions by interacting with the cell surface receptor CD63 [17], altogether rendering TIMP-1 functions strongly context-dependent [12]. While TIMP-1 is overexpressed in lung cancer, whether it interacts with CD63 and how this may contribute to cancer progression remains poorly understood. To address this gap of knowledge, we analyzed the expression of TIMP-1 and its major partner CD63, and investigated the potential tumor-promoting effects of their interaction in NSCLC.

Results

TIMP-1 expression in TAFs and CD63 expression in cancer cells is markedly higher in ADC compared to SCC patients

To analyze the potential role of TIMP-1 and CD63 in NSCLC, we first examined their mRNA levels in whole tumor samples from ADC and SCC patients using the Tissue Cancer Genome Atlas (TCGA) RNA-seq database. Both *TIMP1* and *CD63* mRNA levels were significantly higher in ADC compared to SCC tissue (Fig. 1A-B). Moreover, *TIMP1* mRNA was significantly higher in tumor samples compared to paired control tissue in ADC but not SCC (Fig. 1C-D), whereas *CD63* levels were significantly lower in tumors compared to paired control tissue in SCC but not ADC (Fig. 1E-F). These results reveal an aberrant *TIMP1* and *CD63* expression in NSCLC in which *TIMP1* is overexpressed in ADC and its potential partner *CD63* is downregulated in SCC.

Previous studies have reported TIMP-1 expression in TAFs and cancer cells in lung cancer [18]. To determine which cell type may contribute to *TIMP1* overexpression in ADC, we compared *TIMP1* mRNA between ADC and SCC in a panel of cancer cell lines using the Sanger RNA-seq database and in primary TAFs from our patient cohort (n = 15) by qRT-PCR. All TAFs were activated with TGF-β1 for 3 days to mimic their ubiquitous activated/myofibroblast-like phenotype observed in patient samples [6,19], and are referred to as activated TAFs

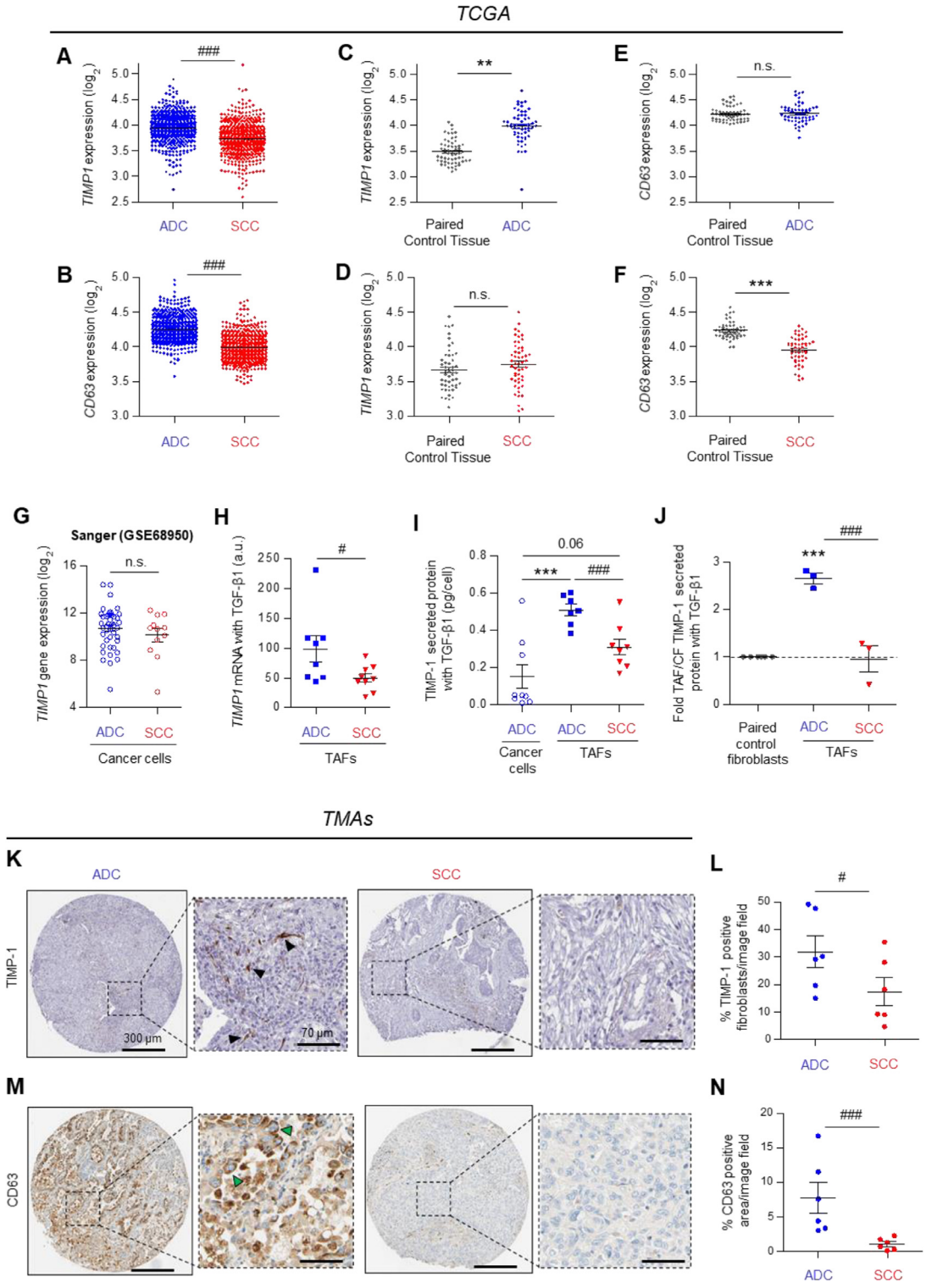

Fig 1. Expression of TIMP-1 and CD63 in lung ADC and SCC. A-F, RNA-seq data of *TIMP1* and *CD63* mRNA in tumoral tissue (A-B) (515 ADC, 501 SCC), in ADC and paired control tissue (C, E) (58 ADC), and in SCC and paired control tissue (D, F) (51 SCC). G, RNA-seq data of *TIMP1* mRNA expression in a panel of lung cancer cell lines (43 ADC, 12 SCC). H, *TIMP1* mRNA level of TAFs (8 ADC, 9 SCC) activated with 2.5 ng/mL TGF-β1 for 3 days (here and thereafter unless otherwise indicated). I, ELISA quantification of TIMP-1 protein (pg of TIMP-1/number of cells) secreted by cancer cells (9 ADC) and TAFs (6 ADC, 8 SCC) activated with 2.5 ng/mL TGF-β1 for 3 days and subsequently maintained in serum-free medium for 2 days. J, Fold (TAF/CF) secretion of TIMP-1 of ADC (n = 3; TAFs and CFs) and SCC (n = 3;

hereafter. *TIMP1* levels were comparable in ADC and SCC cell lines (Fig. 1G), whereas they were significantly higher in activated ADC-TAFs compared to SCC-TAFs (Fig. 1H). Consistently, secreted TIMP-1 protein, as determined by ELISA, was significantly higher in activated ADC-TAFs than in SCC-TAFs as well as in a panel of TGF-β1-stimulated ADC cell lines (Fig. 1I). Moreover, secreted TIMP-1 was significantly higher in TAFs compared to patient-matched control fibroblasts in ADC but not SCC (Fig. 1J), revealing an aberrant overexpression of TIMP-1 selectively in ADC-TAFs.

To independently validate our observed differences between ADC and SCC, we analyzed TIMP-1 and CD63 staining in tissue microarrays (TMAs) from the Human Protein Atlas. In agreement with our initial observations, the percentage of TIMP-1 positive fibroblasts was significantly higher in ADC than SCC (Fig. 1K-L and Supplementary Fig. 1A-B), whereas CD63 staining was very scarce in SCC compared to ADC samples, and was largely restricted to cancer cells (Fig. 1M-N; Supplementary Fig. 1C). Finally, we examined the mRNA and protein expression of MMP9 in patients using the TCGA and Human Protein Atlas databases, respectively, as a potential limiting factor of the interaction between TIMP-1 and CD63, since proMMP9 and CD63 share the same binding domain in TIMP-1 [12]. We found significantly higher MMP9 mRNA levels and tissue staining in SCC compared to ADC tissue (Supplementary Fig. 1D-F), in agreement with previous observations [20,21]. These results reveal that the major cancer cell partner CD63 for free (unbound) TIMP-1 is overexpressed in ADC compared to SCC, whereas its natural competitor MMP9 shows an opposite pattern, thereby strongly supporting that lung ADC tumors are primed for a crosstalk between TIMP-1 in TAFs and CD63 in cancer cells.

TIMP-1 overexpression and secretion in ADC-TAFs is driven by hyperactive TGF-β1/SMAD3 signaling

Prompted by the selective overexpression and secretion of TIMP-1 observed in ADC-TAFs, we began to examine the underlying mechanism(s). The regulation of TIMP-1 secretion is largely unknown. In contrast, TIMP-1 expression is known to be inducible (i.e. not constitutive) [10], and TGF-β1 has been reported as a major inducer of TIMP-1 expression in fibroblasts and other mesenchymal cells [16] and it is frequently upregulated in NSCLC [22]. Accordingly, we examined TIMP-1 expression and secretion in primary TAFs in response to TGF-β1. We observed a greater induction of *TIMP1* mRNA in ADC-TAFs compared to SCC-TAFs with respect to untreated cells (Fig. 2A), and this difference became even larger and statistically significant when analyzing secreted TIMP-1 (Fig. 2B), revealing that ADC-TAFs are hyperresponsive to TGF-β1 in terms of TIMP-1 expression and particularly secretion.

To explore the mechanisms underlying this hyperresponse, we examined the canonical TGF-β1 pathway transcription factor SMAD3, since we recently reported the selective hyperactivity of the TGF-β1/SMAD3 pathway in ADC-TAFs concomitantly with the epigenetic repression of SMAD3 in SCC-TAFs [23]. For this purpose, we used both pharmacologic and genetic loss- and gain-of-function approaches. Stimulating hTERT immortalized primary control pulmonary fibroblasts from a randomly selected patient (CF^{hTERT} (#5), where the number identifies the selected patient henceforth) with the potent SMAD3 inhibitor SB431542 (SB) (Fig. 2C) markedly downregulated *TIMP1* mRNA (Fig. 2D) and secreted levels (Fig. 2E) compared to the weak SMAD3 inhibitor galunisertib [23] (Fig. 2C-E). Consistently, knocking-down SMAD3 in CF^{hTERT} (#5) by shRNA (Fig. 2F) was sufficient to downregulate both TIMP-1 mRNA (Fig. 2G) and secreted levels (Fig. 2H) upon TGF-β1 stimulation compared to shRNA control (shCTRL). Similar results were obtained in CFs derived from a different patient (Supplementary Fig. 2A-C). Conversely, SMAD3 overexpression through retroviral transduction (rv-SMAD3) in CF^{hTERT} (#5) (Fig. 2I) markedly increased basal *TIMP1* mRNA (in the absence of TGF-β1) compared to rv-GFP used as a control (Supplementary Fig. 2D). This transcriptional increase was smaller upon stimulation with TGF-β1 (Fig. 2J), suggesting that *TIMP1* mRNA induction had reached saturation, whereas secreted TIMP-1 was significantly increased in rv-SMAD3 fibroblasts compared to rv-GFP controls (Fig. 2K), identifying SMAD3 as a potent regulator of TIMP-1 secretion. Consistently, we observed a significant correlation between *SMAD3* mRNA and TIMP-1 secretion upon TGF-β1 stimulation in ADC-TAFs (r^2 = 0.84,

TAFs and CFs) fibroblasts cultured as in I. K and M, Representative histologic images of ADC and SCC patient samples within TMAs from the Human Protein Atlas database stained for TIMP-1 (K) and CD63 (M). Black arrowheads point at TIMP-1 positive fibroblasts and green arrowheads point at CD63 positive cancer cells. Additional images in Supplementary Fig. S1A and S1C. L, Percentage of TIMP-1 positive TAFs in TMAs (6 ADC, 6 SCC). N, Quantification of the percentage of CD63-positive area/image field for each patient in TMAs (6 ADC, 6 SCC). Error bars represent mean ± s.e.m. #, $p < 0.05$; ##, $p < 0.01$; ###, $p < 0.005$ comparing ADC with SCC. *, $p < 0.05$; **, $p < 0.01$; ***, $p < 0.005$ comparing with respect to control tissue or CFs. n.s.: non-significant. Statistical comparisons were done using Wilcoxon rank-sum test (A-F) or Student *t*-test (G-N).

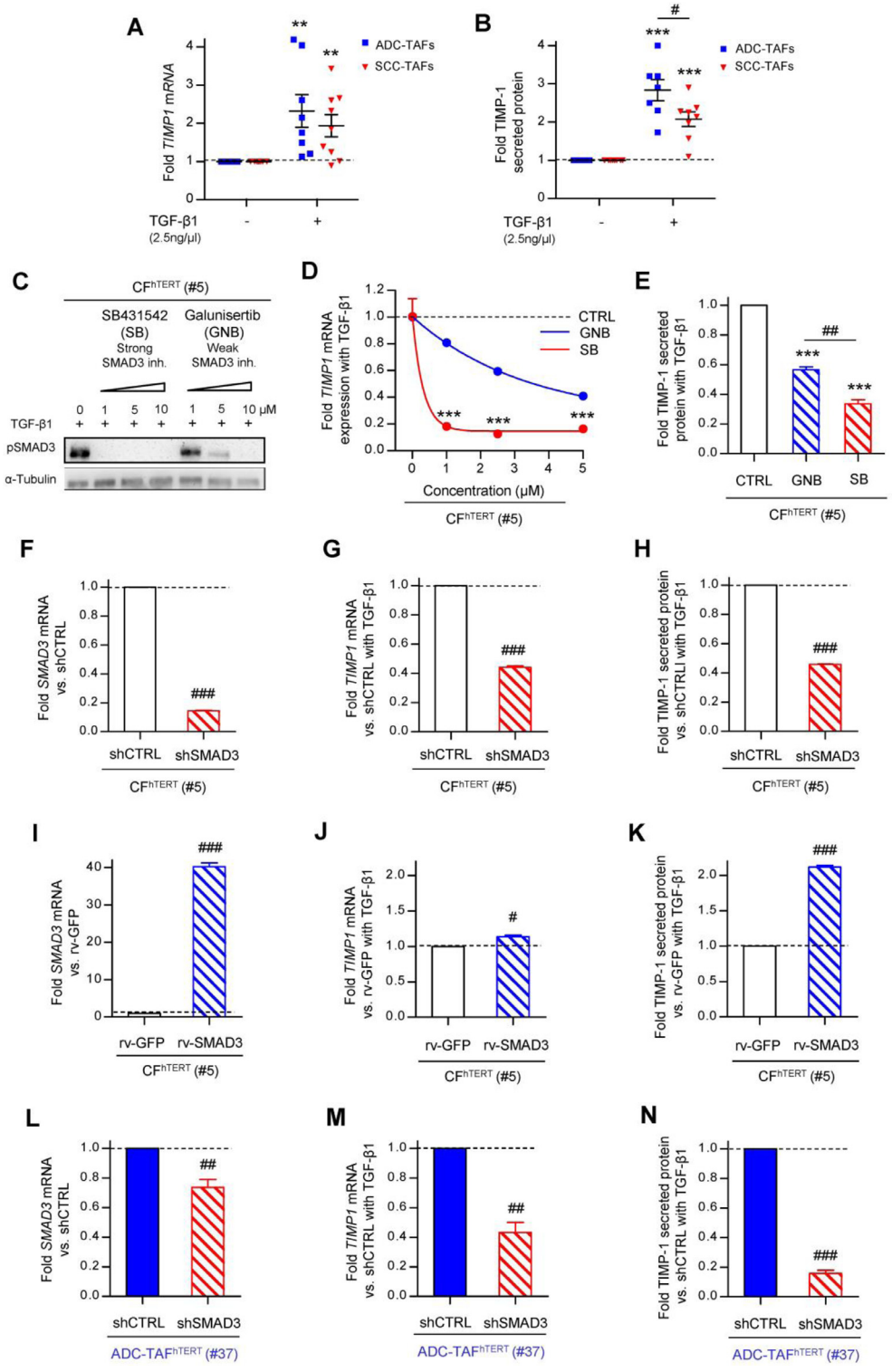

Fig 2. Regulation of TIMP-1 expression and secretion by TGF-β1/SMAD3. A, Fold *TIMP1* mRNA expression of TAFs (8 ADC, 9 SCC) cultured as in Fig. 1H. B, Fold TIMP-1 protein secretion of TAFs (6 ADC, 8 SCC) cultured as in Fig. 1I. C, Representative Western blot for pSMAD3 and α-tubulin of CF^{hTERT} (#5) stimulated with 2.5 ng/mL TGF-β1 for 60 min in the presence of increasing doses of SB431542 or galunisertib. D, Fold *TIMP1* mRNA expression of CF^{hTERT} (#5) cultured as in C. E, Fold TIMP-1 secretion of CF^{hTERT} (#5) stimulated with 2.5 ng/mL TGF-β1 for 3 days alone or in the presence of 2.5μM SB431542 or 2.5μM galunisertib and subsequently maintained in serum-free medium for 2 days. F and L, Fold *SMAD3* expression of shSMAD3 CF^{hTERT} (#5) (F) and $ADC\text{-}TAF^{hTERT}$ (#37) (L) with respect to control shRNA maintained

p = 0.03) (Supplementary Fig. 2E). Lastly, we knocked-down SMAD3 in hTERT immortalized ADC-TAFs from a randomly selected patient (ADC-TAF^{hTERT} (#37)) (Fig. 2L) and found a consistent down-regulation of *TIMP1* mRNA (Fig. 2M) and protein secretion (Fig. 2N).

Both TIMP-1 in ADC-TAFs and CD63 in lung ADC cancer cells are necessary to elicit a tumor-promoting paracrine crosstalk

To examine the functional effects of the potential paracrine interaction between TIMP-1 overexpressing TAFs and CD63 overexpressing cancer cells selectively in ADC, we first knocked-down *TIMP1* in ADC-TAFs by siRNA, activated them with TGF-β1, collected their conditioned medium (CM), and analyzed the CM effect on the growth and invasion of ADC cells as outlined in Fig. 3A. siRNA not targeting any gene product was used as control (siCTRL) here and thereafter. To mimic ADC patients, we selected two ADC cell lines (H1437, H23) exhibiting high surface expression of CD63 (>70%) as determined by flow cytometry (referred to as CD63^{high} ADC cells) (Supplementary Fig. 3A). Knocking-down *TIMP1* in a panel of ADC-TAFs (n = 4 patients) using two constructs (#α and #β) consistently elicited a >90% reduction of secreted TIMP-1 within the CM derived from activated TAFs (Fig. 3B), whereas it did not alter the expression of standard fibrosis markers (Supplementary Fig. 3B-F). In agreement with previous reports [24], the CM of a panel of activated siCTRL ADC-TAFs (n = 4) increased both growth and invasion of ADC cells by ~2-fold in average compared to CM from non-activated TAFs (horizontal dashed line) in both ADC lines (Fig. 3C-F). Moreover, the induction of cancer cell growth and invasion linearly correlated with the amount of secreted (unnormalized) TIMP-1 present within the CM of ADC-TAFs used in each experiment (Supplementary Fig. 3G-J). In contrast, such increase in growth and invasion in ADC cells was significantly attenuated by ~35% (Fig. 3C-D) and ~30% (Fig. 3E-F) on average, respectively, when stimulating cells with CM from activated siTIMP-1 ADC-TAFs, thereby revealing that TIMP-1 is a major contributor to cancer cell growth and invasion in ADC.

Next, we analyzed whether CD63 in ADC cells is also necessary for the TIMP-1-dependent growth and invasion enhancement of the CM of TAFs. For this purpose, we knocked-down *CD63* in ADC cell lines by siRNA using two constructs (#A and #B), which elicited a consistent ~90% reduction in *CD63* mRNA expression (Supplementary Fig. 3 K, L) and in the percentage of CD63 positive cells (Fig. 3G,H). CD63 attenuation did not alter the basal growth of ADC cells (Supplementary Fig. 3 M,O) and increased their basal invasion in one of the constructs in H23 cells (Supplementary Fig. 3 N,P). As expected, the growth and invasion of siCTRL ADC cells markedly increased with the CM of activated ADC-TAFs compared to basal medium (dashed line) (Fig. 3I-L). In contrast, knocking-down CD63 was sufficient to significantly downregulate growth by ~20% in H1437 (Fig. 3I) and ~50% in H23 cells using both constructs compared to either siCTRL (Fig. 3K) or wild-type cells (Supplementary Fig. 4A,B). Likewise, knocking-down CD63 consistently reduced the average invasion elicited by the CM in both cell lines and constructs, although this reduction exhibited more variability and did not attain statistical significance in siRNA#B in H23 cells (Fig. 3J,L). Although the source of this variabillity is unclear, it may be associated with a known function of CD63 to organize the plasma membrane into microdomains with a diverse array of membrane proteins, including integrins and other receptors that may regulate invasion [25]. Therefore, it is possible that different constructs may differentially affect CD63 splice variants and correspondingly lead to differential organization of invasion-relevant proteins within microdomains.

To further implicate TIMP-1/CD63 interaction in a tumor-promoting paracrine crosstalk between ADC-TAFs and CD63^{high} ADC cells, we conducted growth and invasion measurements upon simultaneous downregulation of both proteins. Of note, knocking-down *CD63* in both H1437 and H23 ADC cells (siRNA#A) consistently abrogated the inhibition of growth (Fig. 4A,B right bars) and invasion (Fig. 4C,D right bars) elicited by the CM of activated siTIMP-1 ADC-TAFs compared to the CM of activated parental ADC-TAFs, and comparable findings were obtained with siRNA#B

in fibroblast culture medium supplemented with 10% FBS. G and M, Fold *TIMP1* mRNA of shSMAD3 CF (G) and ADC-TAF (M) with respect to control shRNA fibroblasts cultured as in A. H and N, Fold TIMP-1 secretion of shSMAD3 CF (H) and ADC-TAF (N) with respect to control shRNA fibroblasts cultured as in B. I, Fold *SMAD3* expression of rv-SMAD3 fibroblasts with respect to control rv-GFP fibroblasts maintained as in F. J, Fold *TIMP1* mRNA expression of rv-SMAD3 fibroblasts with respect to control rv-GFP cultured as in B. K, Fold TIMP-1 protein secretion of rv-SMAD3 fibroblasts with respect to control rv-GFP cultured as in B. Similar results were obtained in CFs from other patients (Supplementary Fig. S2). Error bars indicate mean ± s.e.m. **, $p < 0.01$; ***, $p < 0.005$ comparing either TAFs with their respective untreated condition (A) or SB431542 and galunisertib with untreated conditions (D, E). #, $p < 0.05$; ##, $p < 0.01$; ###, $p < 0.005$ comparing either ADC with SCC, shCTRL with shSMAD3 fibroblasts, or rv-GFP with rv-SMAD3 fibroblasts. All comparisons were done using Student t-test. Mean values correspond to $n \geq 2$ experiments.

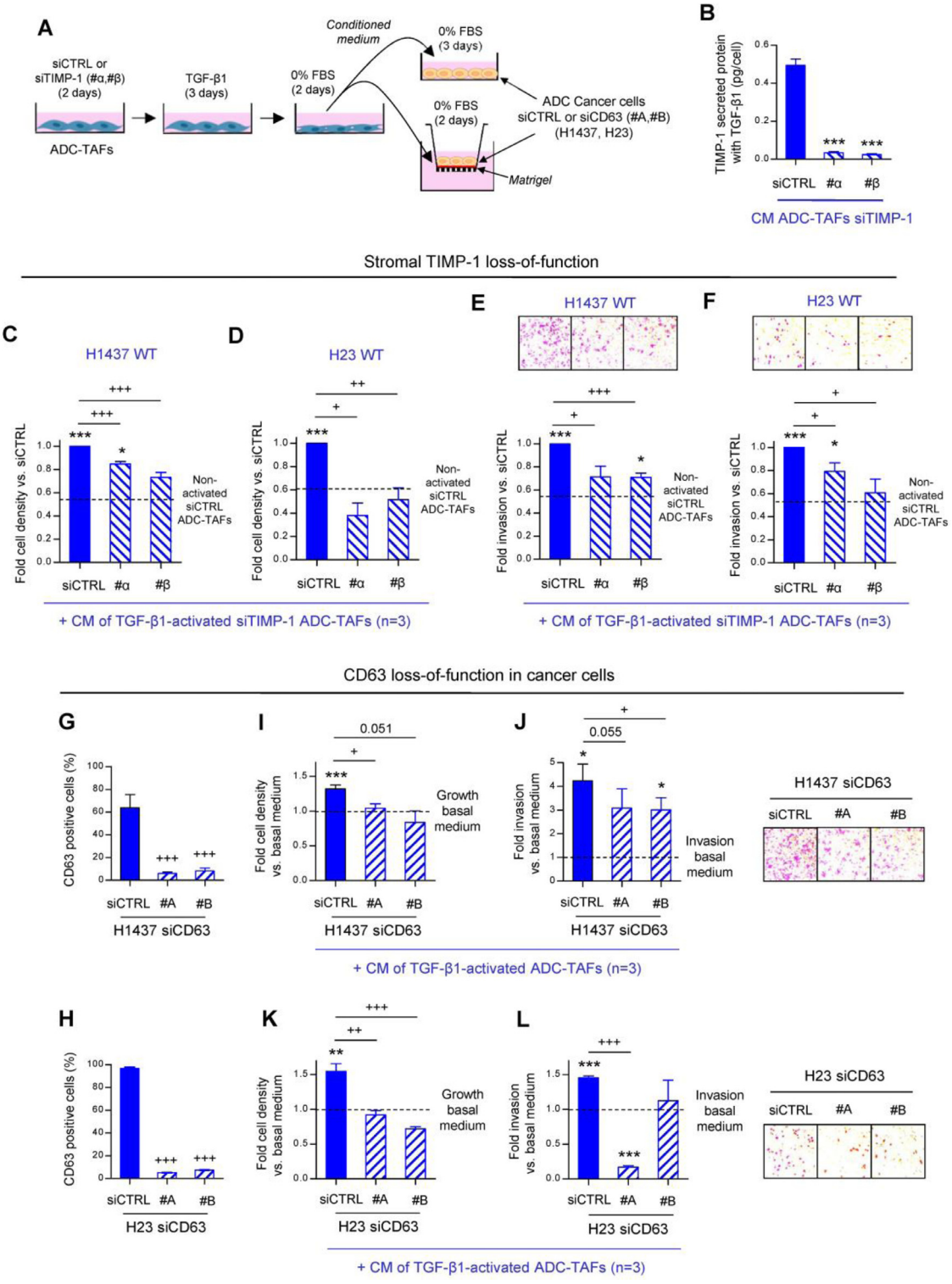

Fig. 3. Tumor-promoting effects of the crosstalk between TIMP-1 in TAFs and CD63 in ADC cells. A, Outline of the experimental design used to assess growth (top right) and invasion (bottom right) of ADC cancer cell lines (siCTRL or siCD63) stimulated with basal medium or CM from ADC-TAFs (siCTRL or siTIMP-1). B, ELISA results of secreted TIMP-1 protein within the CM of activated ADC-TAFs transfected with siTIMP-1 (#α, #β) or siCTRL (n = 4). C-F, Fold cancer cell number density and invasion of H1437 (C and E, respectively) and H23 (D and F) cells stimulated with the CM of siCTRL or siTIMP-1 fibroblasts cultured as in A. Representative images of invading cancer cells are shown above invasion plots. G and H, Percentage of CD63 positive H1437 (G) and H23 (H) cells after transfection with siCD63 (#A, #B) or siCTRL

(Supplementary Fig. 4C-F). These results reveal that TIMP-1 in ADC-TAFs as well as CD63 in ADC cells are both necessary effector proteins of a tumor-promoting paracrine interaction between TAFs and carcinoma cells in ADC. Lastly, to further confirm the specificity of TIMP-1/CD63 interaction in cancer cells, we assessed Akt activation through phosphorylation at serine 473 (Supplementary Fig. 4G), which has been reported as a major tumor-promoting signaling protein downstream of TIMP-1/CD63 crosstalk in different cancer cell types including lung cancer cells [15,16]. As expected, the CM of activated ADC-TAFs significantly increased Akt^{pS473} in H1437 ADC cells (Supplementary Fig. 4H,I), whereas knocking-down *TIMP1* in ADC-TAFs abrogated this increase (Supplementary Fig. 4 J,K).

Stimulation with recombinant TIMP-1 is sufficient to mimic completely the growth and partially the invasion increase elicited by the CM on ADC cells in a CD63-dependent manner

To assess whether TIMP-1 alone is sufficient to increase growth and/or invasion of $CD63^{high}$ ADC cells, we stimulated them with either 10 or 160 ng/mL of recombinant human TIMP-1 (rhTIMP-1), which covered doses used elsewhere [26] and included the average amount of (unnormalized) TIMP-1 secreted by activated ADC-TAFs (Supplementary Fig. 4L). Stimulation with basal medium supplemented with rhTIMP-1 induced a dose-dependent growth increase in both ADC cell lines up to ~20% in average, which was comparable to that attained with the CM of activated TAFs (Fig. 4E,G), revealing that TIMP-1 is a dominant growth-promoting factor within the secretome of TAFs. Notably, rhTIMP-1 elicited an even larger average increase in invasion by ~60% at the higher concentration, though this was a smaller effect than that elicited by the CM of activated TAFs (Fig. 4F,H). These results illustrate that TIMP-1 is a potent invasion inducer of ADC cells, and underscore that TAFs secrete other relevant invasion-inducing factors that remain to be identified. Conversely, knocking-down CD63 significantly attenuated the growth (Fig. 4I,K) and invasion (Fig. 4J, L) enhancement elicited by rhTIMP-1 in both ADC lines. These results reveal that exogenous TIMP-1 is sufficient to increase the growth and invasion of $CD63^{high}$ ADC cells.

Knocking-down SMAD3 or TIMP-1 in fibroblasts coinjected with ADC cells is sufficient to attenuate tumor aggressiveness *in vivo*

To test our observed tumor-promoting role of aberrant SMAD3/TIMP-1 expression of ADC-TAFs *in vivo*, we used two complementary approaches as outlined in Fig. 5A. First, we coinjected subcutaneously H1437 cells with either activated shCTRL or shSMAD3 CF^{hTERT} (#5) and monitored tumor growth for 3 weeks (Fig. 5A; upper left). This relatively short time-window minimizes the expected contribution of host stromal cells [27]. We did not use shSMAD3 ADC-TAF^{hTERT} owing to technical difficulties in expanding this cell population. Alternatively, we coinjected H1437 cells with either siCTRL or siTIMP-1 ADC-TAF^{hTERT} (#37) and monitored tumor growth within the same time-window (Fig. 5A; upper right). We used siRNA rather than shRNA to knock-down TIMP-1 *in vivo* owing to the difficulties in expanding the latter cells as described above; moreover, siTIMP-1 ADC-TAF^{hTERT} (#37) maintained a strong downregulation (>90%) of secreted TIMP-1 in culture throughout the experimental time-window (Fig. 5B). All fibroblasts used in both *in vivo* assays were pre-activated with TGF-β1 for 3 days before coinjection to mimic the profibrotic phenotype of TAFs found in patients.

In agreement with our cell culture observations, tumor growth was significantly lower in tumors coinjected with fibroblasts with reduced SMAD3 (Fig. 5C) by ~60% at the end of the observation period. Similarly, we observed a lower tumor volume in mice bearing siTIMP-1 ADC-TAFs compared to siCTRL (Fig. 5D), confirming the results of an initial pilot study (Supplementary Fig. 5A), although these differences did not reach statistical significance. Yet, combining both independent *in vivo* experiments ($n = 7$ siTIMP-1, $n = 6$ siCTRL) using a linear regression mixed model revealed that the difference between both groups reached marginal significance ($p = 0.08$). Consistently, tumor weight (Fig. 5E, F) was lower in tumors bearing reduced SMAD3 or TIMP-1 compared to controls. The larger drop in tumor growth observed in shSMAD3 compared to siTIMP-1 conditions with respect to their controls could be attributed in part to the marked drop in fibrosis in tumors bearing shSMAD3 but not siTIMP-1 fibroblasts, as illustrated by the distinct deposition of fibrillar collagens as stained by picrosirius red (PSR) (Fig. 5G-J), which is consistent with the major transcriptional regulation of fibrotic genes by

($n \geq 3$). I and K, Fold cell density induction of siCD63 H1437 (I) and siCD63 H23 cells (K) stimulated with the CM of fibroblasts cultured as in A with respect to basal medium. J and L, Fold cell invasion of siCD63 H1437 (J) and siCD63 H23 cells (L) stimulated with the CM of parental fibroblasts cultured as in A with respect to basal medium. Representative images of invading cancer cells are shown right to invasion plots. Error bars represent mean ± s.e.m. *, $p < 0.05$; **, $p < 0.01$; ***, $p < 0.005$ comparing with siCTRL non-activated TAFs (C-F) or basal medium (I-L). +, $p < 0.05$; ++, $p < 0.01$; +++, $p < 0.005$ comparing with corresponding siCTRL. All comparisons were done using Student *t*-test. Mean values correspond to $n = 3$ experiments with samples in duplicates.

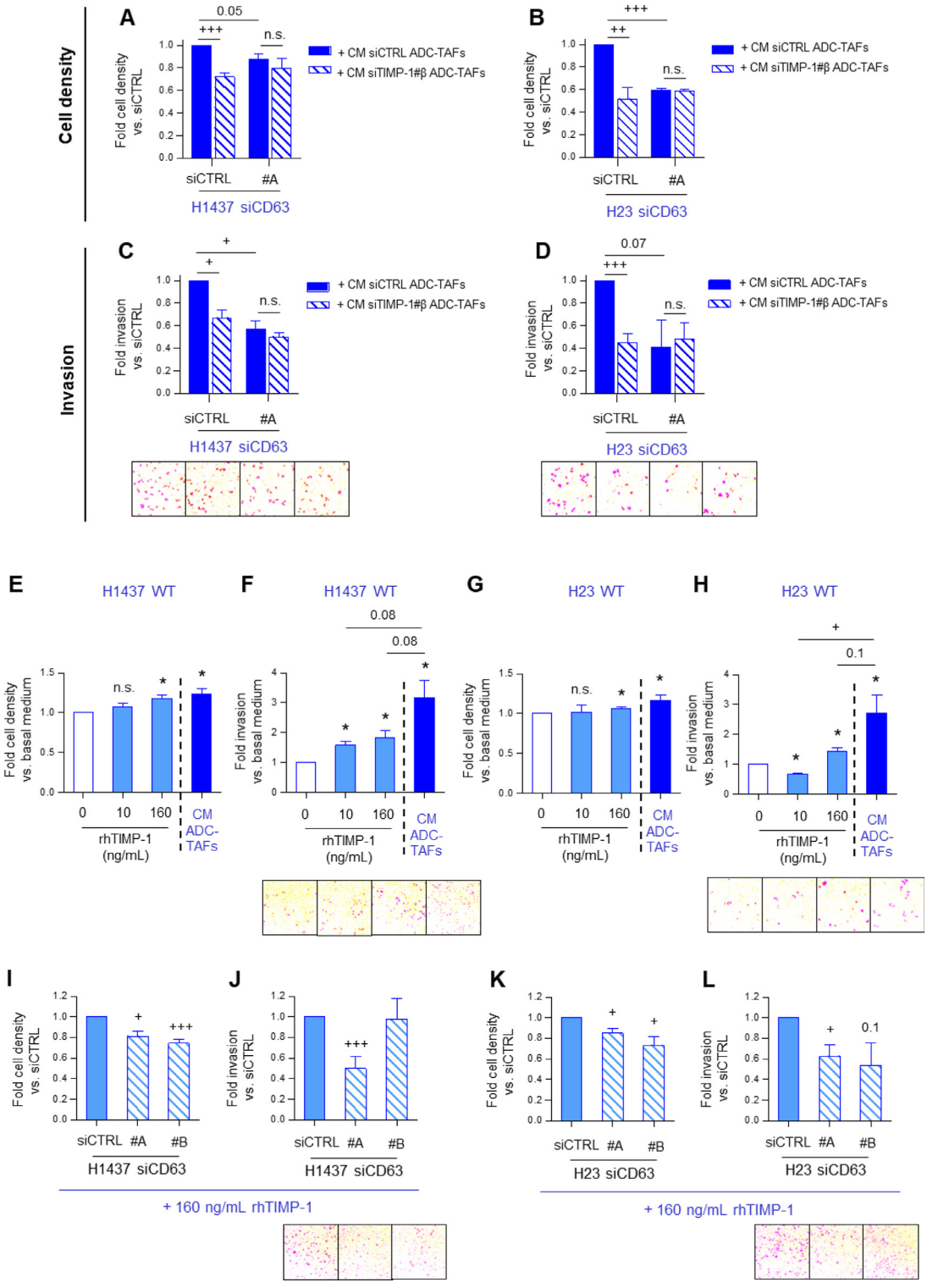

Fig. 4. Effect of either simulatenous knock-down of TIMP-1 in TAFs and CD63 in ADC cell lines or rhTIMP-1 treatment in cancer cell growth and invasion. A and B, Fold cancer cell density of H1437 (A) and H23 (B) transfected with siCTRL (left bars) or siCD63#A (right bars) and stimulated as in Fig. 3A. C and D, Fold cell invasion of H1437 (C) and H23 (D) transfected with siCTRL (left bars) or siCD63#A (right bars) and stimulated as in A. Representative images of invading cancer cells are shown below invasion plots. E and F, Fold cancer cell density (E) and invasion (F) of H1437 stimulated with growing concentrations of rhTIMP-1 (10 and 160 ng/mL) or the CM of ADC-TAFs (n = 4) cultured as in Fig. 1I. G and H, Fold cancer cell density (G) and invasion (H) of H23 stimulated with growing concentrations of rhTIMP-1 (10 and

SMAD3 [28], since a fibrotic stroma provides a wound-like microenvironment that favours tumor progression through both soluble and insoluble factors [3]. In further agreement with the pro-invasive effects of stromal TIMP-1 in culture, knocking-down TIMP-1 in TAFs was sufficient to attenuate the invasion of tumor xenografts to their adjacent host tissue (Fig. 5K-L and Supplementary Fig. 5B, C). These results reveal that reducing the expression of a single stromal factor (i.e. TIMP-1) in TAFs attenuates tumor aggressiveness compared to control conditions, even in the context of a similar collagen-rich fibrotic tumor stroma (Fig. 5H, J).

High combined expression of *TIMP1* and *CD63* is more strongly associated with poor survival than *TIMP1* alone

TIMP-1 is a well-established prognostic biomarker candidate in lung cancer, since high levels of TIMP-1 mRNA or protein have been consistently associated with poor prognosis [18,29]. To examine whether CD63 may increase the prognostic value of TIMP-1, we conducted survival analysis of *TIMP1* and *CD63* mRNA alone or in combination using publicly available databases. As expected, high *TIMP1* was associated with significantly poorer survival in ADC (HR = 3.18; 95% CI, 2.31−4.38; $p = 6.7 \times 10^{-14}$) (Fig. 6A). Likewise, the ADC patient group with high *CD63* mRNA levels also had a poorer prognosis (HR = 2.67; 95% CI, 1.98−3.59; $p = 1.4 \times 10^{-11}$) (Fig. 6B). Notably, the ADC patient group exhibiting high expression of both *TIMP1* and *CD63* mRNA exhibited the highest increased risk of death (HR = 3.53; 95% CI, 2.57−4.87; $p = 1.7 \times 10^{-16}$) (Fig. 6C). These results unveil the potential of combined *TIMP1* and *CD63* as a prognostic biomarker, and underscore the important role of TIMP-1/CD63 crosstalk in ADC. In contrast, none of these mRNA biomarkers exhibited any prognostic value in SCC (Supplementary Fig. 6).

Discussion

Understanding TIMP-1 function and regulation within the tumor microenvironment is drawing increasing attention because it is consistently associated with poor prognosis in virtually all human cancers including NSCLC [11,18,29], and there is growing evidence that TIMP-1 promotes tumor progression in NSCLC [14,15] and other cancer types [16,26,30,31], although there is some inconsistency in the literature on this latter point [32,33]. Similarly, the few previous studies on the role of TIMP-1 in TAFs have reported conflicting results [16,34,35], illustrating collectively the complexity of defining TIMP-1 functions in cancer. In addition, the source of TIMP-1 expression in NSCLC had remained unclear, with some studies favoring stromal expression while others favouring expression in cancer cells [9,18,36]. Our results now show that TIMP-1 is expressed by both stromal and cancer cells but is selectively overexpressed in ADC-TAFs compared to SCC-TAFs. These results are consistent with previous studies reporting higher TIMP-1 in ADC than SCC, although those studies did not identify the underlying effector cell type [37−39]. Mechanistically, our results strongly support that the aberrant TIMP-1 overexpression in ADC-TAFs is largely driven by their recently reported hyperactive TGF-β1/SMAD3 pathway [23] as summarized in Fig. 6D, whereas this pro-fibrotic pathway is markedly attenuated in SCC-TAFs, owing to their epigenetic repression of SMAD3 caused by an excessive exposure to cigarette smoke particles [23]. In addition, our findings reveal a novel function for SMAD3 as a positive regulator of TIMP-1 secretion.

It is increasingly recognized that TIMP-1 may elicit either MMP-inhibitory or cytokine-like effects depending on the context, which may manifest as tumor-protective or tumor-promoting, respectively [12]. In NSCLC, our results strongly support that TIMP-1 secreted by ADC-TAFs exhibits tumor-promoting cytokine-like functions through a paracrine crosstalk with CD63 expressing cancer cells (Fig. 6D). First, we used cell culture and animal models to show that TIMP-1 secreted by ADC-TAFs promotes cancer cell growth and invasion, and that CD63 expression in ADC cells is required to convey these tumor-promoting effects. Second, we showed that CD63 is markedly overexpressed in ADC cells, whereas its natural competitor MMP9 [12] is strongly downregulated in ADC compared to SCC tumors, in agreement with previous observations at RNA [20] and protein level [21]. Third, we found that TIMP-1 expression and secretion were regulated by the TGF-β1/SMAD3 pathway, which is hyperactive selectively in ADC-TAFs [23], further supporting that ADC tumors are primed to exhibit more free (i.e.

160 ng/mL) or with the CM of ADC-TAFs cultured as in Fig. 1I. I and J, Fold cancer cell density (I) and invasion (J) of siCD63 H1437 with respect to siCTRL H1437 cells stimulated with 160 ng/mL of rhTIMP-1. K and L, Fold cancer cell density (K) and invasion (L) of siCD63 H23 cells with respect to siCTRL H23 stimulated with 160 ng/mL of rhTIMP-1. 160 ng/ml is very close to the average amount of TIMP-1 secreted by ADC-TAFs (153 ng/ml, Suppl. Fig 4L). Error bars indicate mean ± s.e.m. ***, $p < 0.005$ comparing with basal medium (E-H). +, $p < 0.05$; ++, $p < 0.01$; +++, $p < 0.005$ comparing with corresponding siCTRL. n.s.: non-significant. All comparisons were done using Student *t*-test. Mean values correspond to $n \geq 3$ experiments.

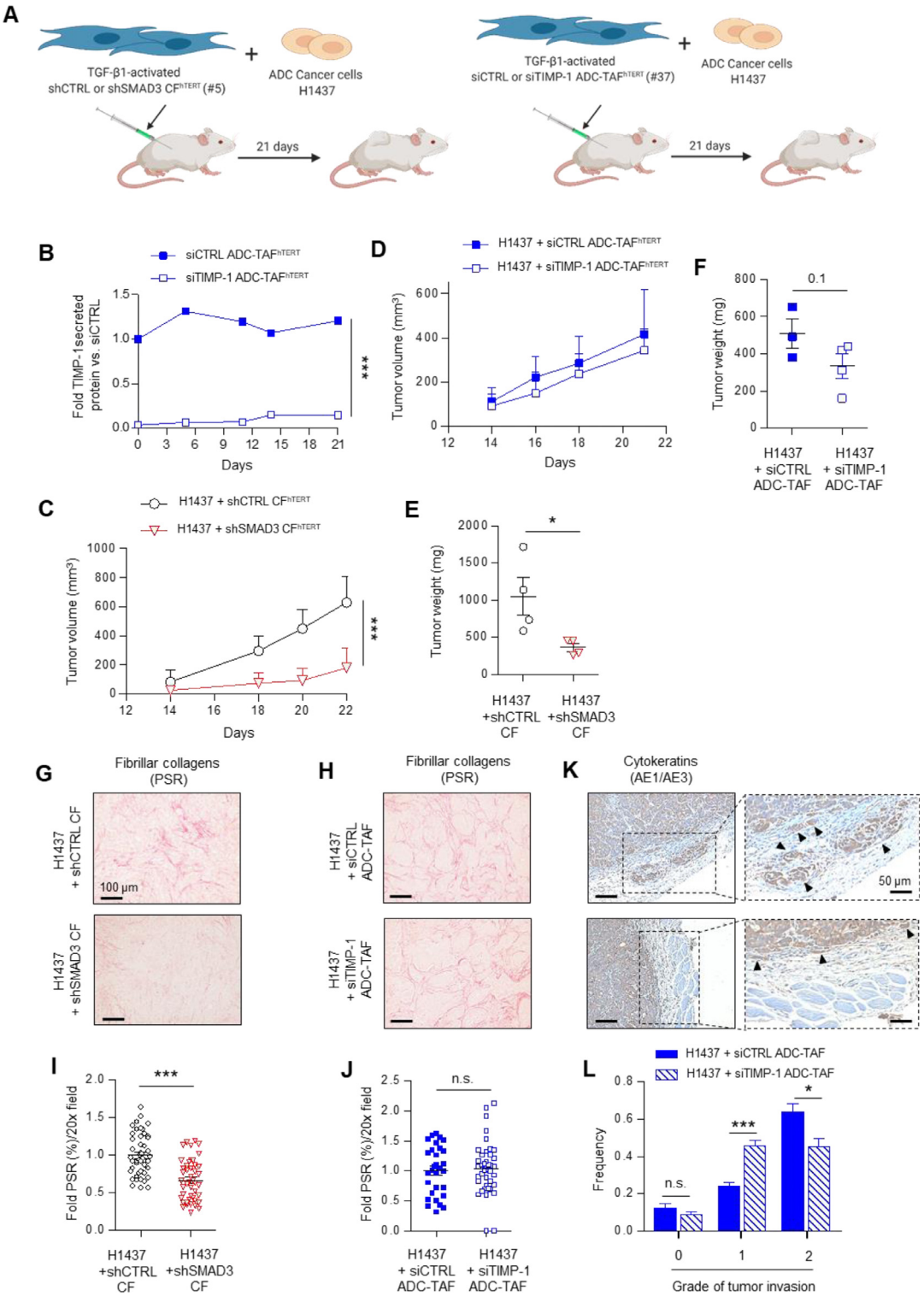

Fig. 5. Role of stromal SMAD3 and TIMP-1 in tumor promotion *in vivo*. A, Outline of the experimental design used to assess tumor growth of H1437 cells subcutaneously co-injected with either shCTRL or shSMAD3 CF^{hTERT} (#5) (2:1 ratio) (upper left), or with siCTRL or siTIMP-1#α ADC-TAF^{hTERT} (#37) (1:1 ratio) (upper right) into immunodeficient NOD/SCID mice (n = 4 mice/condition). Fibroblasts were pre-activated with 2.5 ng/mL with TGF-β1 for 3 days before co-injection (drawings from Biorender). B, Fold TIMP-1 secretion of activated siTIMP-1#α ADC-TAF^{hTERT} (#37) with respect to siCTRL during 21 days after transfection. C and D, Average tumor growth for each experimental condition. E and F, Average tumor weight at the end of the observation period for each experimental condition. G and H, Representative images

proMMP9 unbound) TIMP-1 that can interact with CD63 expressing cancer cells compared to SCC. Finally, the combination of high *TIMP1* and *CD63* tissue mRNA exhibited a stronger prognostic value than *TIMP1* mRNA alone in ADC.

Our *in vitro* observations using recombinant TIMP-1 revealed a differential role in growth and invasion, since TIMP-1 *per se* was sufficient to fully match the growth enhancement elicited by the CM of ADC-TAFs, whereas it only partially matched the invasion increase of the CM, revealing that ADC-TAFs secrete other relevant invasion-inducing factors that remain to be identified. Unlike ADC, the effects of stromal TIMP-1 in SCC remain obscure. Yet, it is possible that TIMP-1 may function primarily to inhibit MMPs rather than eliciting cytokine-like functions in SCC, since the expression of CD63 was low whereas that of its competitor MMP9 was high compared to ADC. In addition, since TIMP-1 expression was markedly lower in SCC-TAFs compared to ADC-TAFs, it may be that there is comparatively less free TIMP-1 in SCC, which is required for its tumor-promoting cytokine-like functions [10]. Alternatively, a previous study on TIMPless fibroblasts reported a tumor-promoting phenotype through the aberrant secretion of exosomes and an enhanced induction of epithelial-mesenchymal transition [34], which could apply to the low TIMP-1 conditions of SCC reported here.

Intriguingly, we observed a significant downregulation of CD63 selectively in lung SCC, and that forcing CD63 downregulation in ADC cells (mimicking SCC conditions) elicited a phenotype that was overall less responsive to the tumor-promoting cues elicited from ADC-TAFs. Yet, we previously reported that activated SCC-TAFs enhance growth and invasion of SCC cells [24], supporting that SCC-TAFs drive tumor progression through molecular mechanisms that are fundamentally different than ADC. Regarding the causes of the differential CD63 expression in ADC and SCC, it is worth noting that, in physiologic pulmonary conditions, CD63 is expressed in pneumocytes and airway epithelium [40]. Thus, the elevated *CD63* expression in ADC reported here may reflect the retention of increased numbers of differentiated epithelial cells in this tumor type. In contrast, it has been suggested that the low CD63 expression in SCC may be due to the negative CD63 expression of basal cells, since SCC tumors are thought to arise from basal stem cells [2,41]. Defining the effects of low CD63 in SCC remains to be determined. Conversely, our work supports that the high CD63 expression in ADC cells contributes to tumor progression through a paracrine interaction with stromal TIMP-1 (Fig. 6D).

Our results unveil that TAF-carcinoma interactions may strongly depend on the histologic subtype by identifying the first paracrine interaction that is specific for lung ADC, unlike previous studies that analyzed tumor-promoting factors secreted by lung TAFs without considering their histologic subtype [37–39]. In addition, our work suggests that TIMP-1/CD63 crosstalk in lung ADC may be suitable for therapeutic intervention. Because the pro-fibrotic TGF-β1/SMAD3 pathway drives TIMP-1 overexpression in ADC-TAFs, it is conceivable that antifibrotic drugs may help inhibiting TIMP-1 in ADC. In support of this possibility, the antifibrotic drug nintedanib [23], which was clinically approved in lung ADC owing to the LUME-1 clinical trial reporting therapeutic benefits selectively in ADC but not SCC [42], was shown to reduce TIMP-1 expression in a mouse model of pulmonary fibrosis [43]. Unlike TIMP-1, the suitability of directly targeting CD63 is unclear, since both high and low CD63 expression have been associated with tumor promotion [44,45]. Therefore, our work supports future efforts towards developing therapeutic strategies against TIMP-1 in ADC and other cancer types exhibiting a prominent fibrotic stromal microenvironment.

In summary, our work provides compelling evidence supporting that ADC tumors are selectively primed for a tumor-promoting TAF-carcinoma crosstalk through TIMP-1/CD63, underscoring its potential as a novel therapeutic target. Moreover, we identify the hyperactive TGF-β1/SMAD3 pathway as a major driver of the aberrant TIMP-1 expression and secretion in ADC-TAFs within the tumor microenvironment, and report high *TIMP1* and *CD63* tissue mRNA as a prognostic biomarker candidate in ADC.

Experimental procedures

Patient-derived lung fibroblasts

Primary fibroblasts were previously derived as tissue explants from a cohort of 20 NSCLC surgical

of picrosirius red (PSR) staining at the end of the observation period of shSMAD3 (G) and siTIMP-1 (H) tumors. I and J, Quantification of the fold percentage of the PSR-positive area of shSMAD-3 (I) and siTIMP-1 (J) tumors for each image and mice ($n \geq 10$ images/tumor). K, Representative images of the tumor edge of pan-cytokeratin staining with AE1/AE3 . Arrow heads indicate invasive tumor nests. Additional images in Supplementary Fig. S5B. L, Frequencies of tumor invasion scores assessed from each AE1/AE3 staining image (10 images/tumor in average). Correlation between frequencies assessed from two observers shown in Supplementary Fig. S5C. Error bars indicate mean ± s.d. (C and D) or ± s.e.m. (E-L). *, $p < 0.05$; ***, $p < 0.005$; comparing either shCTRL with shSMAD3 or siCTRL with siTIMP-1. n.s.: non-significant. Two-group comparisons within time-dependent TIMP-1 or tumor growth data were performed with a linear regression mixed model with random effects model. All other group comparisons were conducted using Student *t*-test.

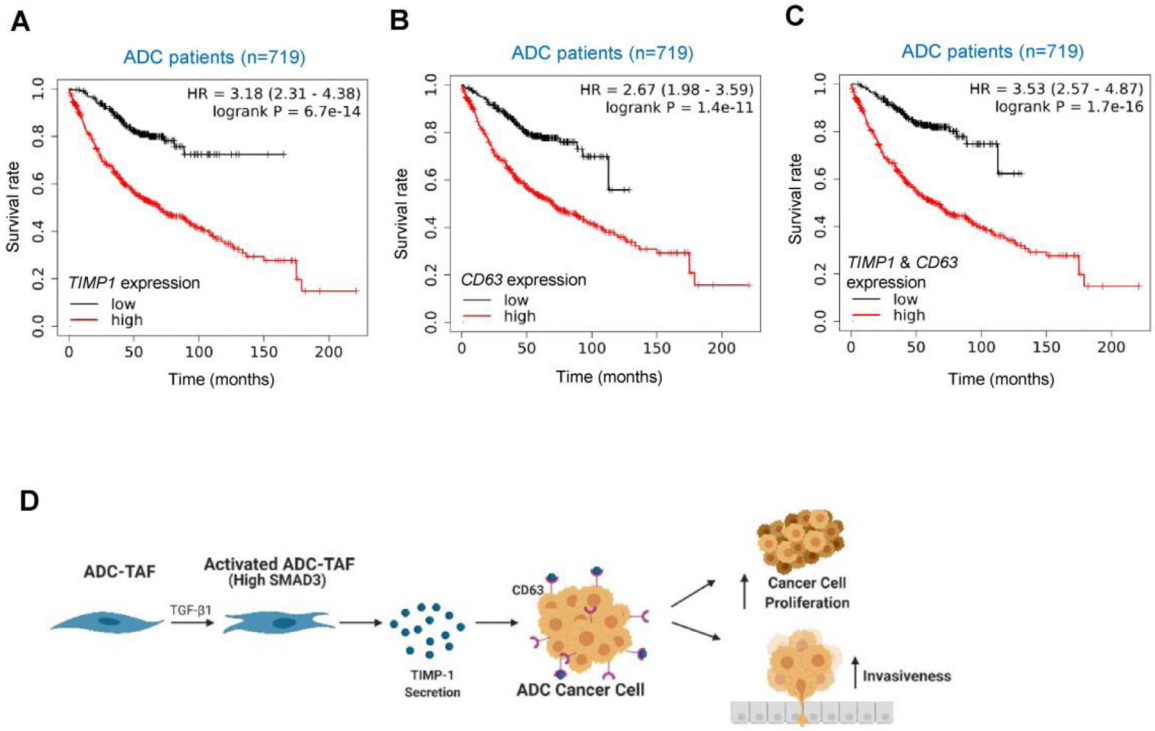

Fig. 6. Prognostic value of *TIMP1* and *CD63* mRNA in lung ADC. A and B, Kaplan-Meier survival curves stratifying patients according to *TIMP1* (A) and *CD63* (B) expression. C, Kaplan-Meier survival curve stratifying patients according to *TIMP1* and *CD63* co-expression. Survival curves were compared by log-rank test. D, Emerging model of the tumor-promoting role of the aberrant SMAD3/TIMP-1 expression of ADC-TAFs with CD63 expressing ADC cells (drawings from Biorender).

patients (8 ADC, 12 SCC) [6]. Fibroblasts were obtained from either tumor or paired-uninvolved pulmonary tissue (used as control fibroblasts (CFs)) with the informed patient consent, using protocols approved by the Ethics Committee of the *Hospital Clinic de Barcelona* and the *Universitat de Barcelona* (clinical characteristics in Supplementary Table S1).

Recombinant human TIMP-1 (rhTIMP-1) production

Mature secreted full-length rhTIMP-1 was obtained by expressing the pTT/TIMP-1 construct transfected into HEK 293E cells [46], and purifying it with SP-Sepharose chromatography as described [47].

Cell culture and fibroblast immortalization

Fibroblast experiments were performed on fibroblast culture medium containing serum-free high-glucose DMEM supplemented with 1% ITS and antibiotics as reported [24]. Unless otherwise indicated, all fibroblasts were treated with 2.5 ng/mL recombinant human TGF-β1 (R&D systems) for 3 days to regain the activated phenotype observed in patient samples [6,19], which is partially lost in culture [5]. This concentration is comparable to the average TGF-β1 concentration reported in the bronchoalveolar lavage fluid of lung cancer patients [48]. In some experiments, fibroblasts were stimulated with TGF-β1 in the presence of 2.5 μM SB431542 (Millipore) or 2.5 μM galunisertib (Lilly, provided by Kyla Driscoll). Fibroblasts from randomly selected patients were immortalized with hTERT transduced expression as reported [23]. A panel of lung carcinoma cell lines derived from ADC patients (H1437, H23, H522, H1975, H441, H2126, H1792 and HCC827) (ATCC) were used for TIMP-1 ELISA analysis. H1437 and H23 were also used in growth and invasion assays. Cancer cells were cultured in a RPMI-based culture medium as described [24]. Cells were routinely tested for mycoplasma contamination as reported [23].

Knock-down of SMAD3 or TIMP-1 in fibroblasts, and of CD63 in cancer cells

SMAD3 was stably knocked-down in immortalized CFs or ADC-TAFs with lentiviral shRNA transduction as reported [23]. TIMP-1 was transiently knocked-down in immortalized ADC-TAFs with siRNA as follows. ADC-TAFs at 30−50% confluency were transfected with 30 nM of two TIMP-1 Silencer Select pre-designed siRNA constructs (12759

TIMP-1#α; 118687 TIMP-1#β) and the Silencer Select negative control No.1 siRNA construct (Thermofisher Scientific) using Lipofectamine RNAiMAX. 48 h after transfection, culture medium was washed and replaced with serum-free fibroblast culture medium supplemented with 2.5 ng/mL TGF-β1 for 3 days. Next, culture medium was replaced with serum-free fibroblast culture medium for 48 h. Afterwards the CM was collected, centrifuged to remove suspended cells and stored at −80 °C until use. Likewise, CD63 was transiently knocked-down in ADC cell lines (H1437 and H23) by siRNA. To this aim, ADC cells at 50−80% confluency were transfected with 30 nM of two CD63 Silencer Select predesigned siRNA constructs (10318 CD63#A; 145984 CD63#B) and the Silencer Select negative control No.1 siRNA construct (Thermofisher Scientific) using Lipofectamine RNAiMAX. Growth and invasion induction by CM or rhTIMP-1 were analyzed in cells 24 h after transfection.

Overexpression of SMAD3 in fibroblasts

SMAD3 was stably introduced in immortalized CFs with retroviral expression vectors. For this purpose, bacteria containing plasmids for SMAD3 (#12638) [49] and GFP (#65436) [50] expression (Addgene) were used. First, bacteria were grown overnight in LB medium (Sigma-Aldrich) containing ampicillin antibiotic (Sigma-Aldrich) and then had their plasmids extracted by QIAGEN plasmid maxi prep kits (#12181) following manufacturer's protocol. Second, Phoenix Ampho cells (ATCC) were seeded in 100 mm plates at 70% confluence and transfected with SMAD3 or GFP plasmids using the CalPhos Mammalian Transfection kit (#631312, Clontech Laboratories) following manufacturer's protocol. Medium containing retroviruses for protein expression was collected, centrifuged and filtered using 0.45um filters (GVS filter technology). Fibroblast transduction was performed using polybrene (Sigma #107689). Cells transduced with retrovirus containing either GFP (rv-GFP) or SMAD3 (rv-SMAD3) plasmids were selected with puromycin (Sigma).

Conditioned medium (CM)

CM of activated fibroblasts was obtained as reported [24]. In brief, fibroblasts (6 CFs, 7 ADC and 8 SCC) were activated with 2.5 ng/mL TGF-β1 for 3 days in serum-free fibroblast culture medium, and subsequently kept in serum-free medium for 2 days in the absence of exogenous TGF-β1. The corresponding CM was collected and the number of cells/mL were counted for normalization. The same protocol was applied to collect CM of ADC cell lines, using serum-free epithelial culture medium.

qRT-PCR

RNA extraction and reverse transcription were conducted as reported [24]. In brief, *TIMP1* and *CD63* mRNA were assessed by qRT-PCR in technical duplicates with the StepOnePlus Real-Time PCR System (Applied Biosystems) using Taqman probes for *TIMP1* (#Hs00171558_m1), *CD63* (#Hs01041238_g1), *COL1A1* (#Hs00164004_m1), *COL3A1*(#Hs00943809_m1) and *POL2R* (#Hs00172187_m1, used as endogenous control) and Taqman Master Mix (ThermoFisher). *SMAD3* mRNA analysis was conducted as described [23]. Relative gene expression with respect to the housekeeping gene/endogenous control was assessed as $2^{-\Delta Ct}$ [51].

Western blot

Protein extraction was performed with a lysis buffer containing Tris 50 mM pH 7.4, NaCl 150 mM, SDS 0.1%, Triton X-100 1% (Sigma), Nonidet P-40 1% (Igepal), proteinase (Cocktail Set I, Merck; Pefabloc, Roche), and phosphatase (Phostop, Roche) inhibitors. Equal protein amounts were separated with precast gels, transferred to a polyvinylidene difluoride membrane as described [23], blocked, and incubated overnight with primary antibodies against phosphorylated SMAD3 (pSMAD3) (#07−1389, Merck Millipore) and α-Tubulin (#2144, Cell Signaling Technology; used as loading control) as well as against P4HA2 (#13,758−1-AP, Proteintech), α-SMA (#A5228, Sigma-Aldrich), Akt^{pS473} (#4060S), Akt (#9272S, Cell Signaling) and β-Actin (#A1978, Sigma-Aldrich; used as loading control). Protein bands were labeled and visualized by chemiluminescence (Chemidoc Imaging Systems, Bio-Rad). Band intensities were analyzed with ImageJ and normalized to the corresponding loading control. Since pAkt and Akt have the same molecular weight (60 kDa), samples were loaded in two independent precast gels and ran in parallel; α-Tubulin levels were assessed as a loading control (referred to as $\alpha\text{-Tubulin}^{(1)}$ in the "pAkt membrane" and $\alpha\text{-Tubulin}^{(2)}$ in the "total Akt membrane"). To obtain the final pAkt/Akt ratio, the $pAkt/\alpha\text{-Tubulin}^{(1)}$ densitometry ratio was divided with the corresponding $Akt/\alpha\text{-Tubulin}^{(2)}$ ratio.

Elisa

Commercial DuoSet Human ELISA kit (R&D Systems) was used to measure secreted TIMP-1 protein within the CM as pg/mL in technical duplicates following manufacturer's instructions, which was normalized by the number of cells/mL to assess final TIMP-1 as pg/cell.

Flow cytometry analysis of CD63

Parental or siCD63 ADC cell lines (H1437, H23) were trypsinized and cell suspension was incubated with 10 μg/mL anti-CD63 monoclonal antibody (ab8219, Abcam) for 30 min, subsequently tagged with alexa fluor 488 conjugated goat anti-mouse IgG (A-11029, Invitrogen) for 30 min and fixed with PBS 2% paraformaldehyde for 15 min. Labeled cells were analyzed in biological duplicates with a FACS Canto II cytometer using FACS Diva 5.5 software (BD Biosciences).

Cancer cell growth and invasion

The effect of the CM on cancer cell growth and invasion was assessed in biological triplicates as described [24]. In brief, to assess cancer cell growth, cancer cells were stimulated with CM or a mixture of serum-free fibroblast culture medium and epithelial culture medium (1:1) (referred to as basal medium) for 3 days, and their nuclei were fluorescently stained and counted to measure cell density as the average nuclear density/image. To assess cell invasion we used the Matrigel Transwell invasion assay, in which CM or basal medium was added to the lower Transwell compartment and cancer cells that invaded the Matrigel (BD Biosciences) layer through the other side of the Transwell porous membrane were stained with crystal violet and quantified as positive crystal violet staining area/image. In some experiments, 10 or 160 ng/mL rhTIMP-1 were added to the basal medium. All image analysis was carried out with Image J [52] hereafter.

In vivo tumorigenicity

The tumorigenicity of ADC cancer cells mixed with fibroblasts with either SMAD3 or TIMP-1 downregulation was examined in 4- to 6-week-old male NOD/SCID mice (Janvier) using protocols approved by the Animal Care and Ethics Committee of the University of Barcelona as reported [23]. All fibroblasts were preactivated with 2.5 ng/mL TGF-β1 for 3 days before coinjection. H1437 cells (0.5×10^6) were mixed with either shCTRL or shSMAD3 CF^{hTERT} (#5) (1×10^6) within 100 μL solution of Matrigel mixed with type I collagen (IAC-50, Koken) (1:1) and coinjected subcutaneously in the dorsal flank of NOD/SCID mice. Alternatively, H1437 cells (1×10^6) were mixed with either preactivated siCTRL or siTIMP-1 ADC-TAF^{hTERT} (#37) (1×10^6) and coinjected subcutaneously into NOD/SCID mice using the same protocol. Tumor growth was assessed as $0.5 \times width^2 \times length$ using calipers [53]. After 21 days, animals were euthanized, and tumor xenografts were collected and weighted [23].

Histologic analysis

TMA images of NSCLC patients stained for TIMP-1, CD63 and MMP-9 (5−6 ADC, 4−6 SCC) were downloaded from the Human Protein Atlas database for image analysis [54]. Primary tumor xenografts obtained from *in vivo* studies were processed as described [23] and stained for picrosirius red (PSR) [23] and cytokeratins (AE1/AE3 anti pan-keratin antibody cocktail, Diagnostic Biosystems). Image analysis was carried out under the guidance of our pathologists (JR, CT). TIMP-1 staining in fibroblasts was scored blind by two independent observers. The percentage of TIMP-1 positive fibroblasts/image field was assessed for each observer and averaged to render the final percentage in ADC and SCC. CD63 and PSR positive stained area/image field was assessed as reported [19]. Invasion of cytokeratin-positive cancer cells within tumor xenografts into adjacent mouse host tissue was scored semi-quantitatively by examining tumor budding, which is defined as the presence of isolated small tumor nests in the stroma of the invasive tumor edge [55]. For this purpose, ∼10 images of the tumor edge in AE1/AE3 staining were randomly acquired with a bright-field microscope (BX43) coupled to a digital camera (DP72) using *a* × 20 objective (Olympus). Invasive features (i.e. tumor nests) at the tumor edge were counted blind for each image by two independent observers, and scored into 3 categories: 0 (negative), 1 (weak, < 7 tumor nests, with a clear pseudocapsule), and 2 (strong, ≥ 7 tumor nests, usually without a clear pseudocapsule). The pseudocapsule corresponds to the reactive stromal host tissue that tends to encapsulate the tumor [56]. For each sample, the frequency of each score n_i (where i corresponds to score 0, 1 or 2) was computed as n_i/N (where N is the total number of images) and averaged across the two observers to render the final score frequencies. A good agreement on invasion scores was found for each category and observer (coefficient of correlation $r^2 = 0.9$).

TCGA data analysis

TIMP1 and *CD63* mRNA were analyzed from TCGA data as described [23]. In brief, level 3 RNA-seq expression data for tumor and normal tissue from the TCGA database (https://cancergenome.nih.gov/) was analyzed using the limma package [57] in R (version 3.5.3; http://www.R-project.org/).

Gene expression analysis of cell lines using the Sanger database

TIMP1 mRNA was analyzed in a panel of cell lines (43 ADC, 12 SCC) (Supplementary Table S2) using the publicly available gene expression microarray

dataset from Sanger Cell Line Project (GSE68950) with the CellExpress system [58] as reported [53].

Survival analysis

Survival analysis was carried out with The Kaplan-Meier plotter (KM plotter) website (http://kmplot.com/analysis/), which uses mRNA expression data and relapse free and overall survival information from GEO, EGA and TCGA databases [59]. For *TIMP1* and *CD63* analyses only JetSet best probes were used. For multiple gene analysis, the mean mRNA expression of the selected probes was calculated and used by the program. To analyze the prognostic value, patient samples were split into two groups (high and low expression) according to the best cut-off calculated by the KM plotter, and the Kaplan-Meier survival plots with hazard ratio (HR), 95% confidence intervals (CI) and log-rank *p*-values were obtained.

Statistical analysis

Two-group comparisons were performed with two-tailed Student *t*-test unless otherwise indicated (GraphPad Prism v5.0.). The degree of linear association between ELISA (pg TIMP-1/cell) and qRT-PCR (*SMAD3* mRNA) data were analyzed through the Pearson correlation coefficient (SigmaPlot). The time-dependent secreted TIMP-1 protein data and tumor volume data from independent experiments were analyzed by fitting a linear regression mixed model with random effects using the *nlme* R package (version v4.1.3; http://www.R-project.org/). The significance of the fixed effects was assessed using the likelihood ratio test. A combined analysis of two independent *in vivo* experiments with siTIMP-1 fibroblasts was also conducted using a linear regression mixed model with random effects including the experimental origin as a covariate to obtain adjusted estimates. Statistical significance was assumed at $p < 0.05$. All data shown are mean ± s.e.m. unless otherwise indicated.

Declaration of Competing Interest

The authors declare no competing interests.

Author Contributions

Conceptualization: P. Duch, J. Alcaraz

Methodology: P. Duch, R. Ikemori, N. Díaz-Valdivia, M. Gabasa, J. Alcaraz

Investigation: P. Duch, R. Ikemori, N. Díaz-Valdivia, M. Arshakyan, M. Gabasa, C. Teixidó, J. Ramírez, P. Bragado, C. Fillat, N. Reguart

Formal analysis: P. Duch, R. Ikemori, N. Díaz-Valdivia, M. Arshakyan, M. Gabasa, C. Teixidó, J. Ramírez, N. Reguart, D. Radisky, J. Alcaraz

Writing (original draft): P. Duch, H. Mori, D. Radisky, J. Alcaraz

Administration and resources: E. Radisky, H. Mori, P. Bragado, S. Gea-Sorlí, A. Mateu-Bosch, C. Teixidó, C. Fillat, J. Alcaraz

Funding acquisition: E. Radisky, C. Fillat, N. Reguart, J. Alcaraz

Supervision: P. Duch, P. Bragado, N. Reguart, D. Radisky, J. Alcaraz

Writing (review & editing): M. Gabasa, N. Díaz-Valdivia, P. Bragado, C. Fillat, N. Reguart

Acknowledgements

We thank Lara Sedó, Josep Marimón (CCiTUB), Èlia Alcañiz, Leire Pedrosa, Núria de-la-Iglesia, Isabel Crespo, Sara Ozcoz, Patricia Fernández, Gemma Fuster (IDIBAPS), Kyla Driscoll (Eli Lilly), Isaac Almendros, Bryan Falcones, Esther Marhuenda, Francisco J Fernández-Porras, Patricia Fernández, Alejandro Llorente (UB), Dobryna Zalvidea (IBEC), Daniel Martínez and Elba Marín (Hospital Clínic) for technical support, and Pere Gascón, Daniel Navajas, Ramon Farré (UB) and Xavier Trepat (IBEC) for support. This work was further supported by grants from the Agencia Estatal de Investigación (AEI/FEDER) (PI13/02368, SAF2016−79527-R and PID2019−110944RB-I00 to JA, PI16/00890 to NR, BIO2017−89754-C2−2R to CF), Fundació Privada Cellex (to JA), U.S. National Institutes of Health (grants R01 GM132100 and R01 CA258274 to E.S.R.), Generalitat de Catalunya (AGAUR SGR 661 and CERCA Programme to JA), Junta Provincial de Barcelona de l'Associació Espanyola Contra el Càncer (AECC B16−917 to JA), Sociedad Española de Neumología y Cirugía Torácica − SEPAR (SEPAR 437 to NR), and by fellowships from Ciência sem Fronteiras CNPq (to RI), CONICYT (to NDV) and Universitat de Barcelona/beca APIF (to PD).

Supplementary materials

Supplementary material associated with this article can be found, in the online version, at doi:10.1016/j.matbio.2022.06.009.

Received 14 October 2021;
Received in revised form 10 June 2022;

Accepted 29 June 2022
Available online 2 July 2022

Keywords:
Cancer-associated fibroblast;
Tumor microenvironment;
Fibrosis;
TIMP-1;
CD63;
TGF-β1;
SMAD3

Abbreviations:
ADC, adenocarcinoma; ECM, extracellular matrix; HR, hazard ratio; MMPs, matrix metalloproteinases; NSCLC, non-small cell lung cancer; PSR, picrosirius red staining; rhTIMP-1, recombinant human TIMP-1; SCC, squamous cell carcinoma; TAFs, tumor-associated fibroblasts; TCGA, Tissue Cancer Genome Atlas; TGF-β1, transforming growth factor beta 1; TIMP-1, tissue inhibitor of metalloproteinase 1; TMA, tissue microarray

References

[1] R.L. Siegel, K.D. Miller, A. Jemal, Cancer statistics, 2019, CA Cancer J. Clin. 69 (1) (2019) 7–34.
[2] Z. Chen, C.M. Fillmore, P.S. Hammerman, C.F. Kim, K.-.K. Wong, Non-small-cell lung cancers: a heterogeneous set of diseases, Nat. Rev. Cancer 14 (8) (2014) 535–546.
[3] R. Kalluri, The biology and function of fibroblasts in cancer, Nat. Rev. Cancer 16 (9) (2016) 582–598.
[4] J. Alcaraz, R. Ikemori, A. Llorente, N. Díaz-Valdivia, N. Reguart, M. Vizoso, Epigenetic reprogramming of tumor-associated fibroblasts in lung cancer: therapeutic opportunities, Cancers (Basel) 13 (15) (2021).
[5] M. Vizoso, M. Puig, F.J. Carmona, M. Maqueda, A. Velásquez, A. Gómez, A. Labernadie, R. Lugo, M. Gabasa, L.G. Rigat de Brugarolas, X. Trepat, J. Ramírez, N. Reguart, S. Morán, E. Vidal, A. Perera, M. Esteller, J. Alcaraz, Aberrant DNA methylation in non small cell lung cancer associated fibroblasts, CarcinogenesisCarcinogenesis 36 (2015) 1453–1463.
[6] M. Puig, R. Lugo, M. Gabasa, A. Gimenez, A. Velasquez, R. Galgoczy, J. Ramirez, A. Gomez-Caro, O. Busnadiego, F. Rodriguez-Pascual, P. Gascon, N. Reguart, J. Alcaraz, Matrix stiffening and beta(1) integrin drive subtype-specific fibroblast accumulation in lung cancer, Molecular Cancer Res. 13 (1) (2015) 161–173.
[7] A. Soltermann, V. Tischler, S. Arbogast, J. Braun, N. Probst-Hensch, W. Weder, H. Moch, G. Kristiansen, Prognostic significance of epithelial-mesenchymal and mesenchymal-epithelial transition protein expression in non-small cell lung cancer, Clin. Cancer Res. 14 (22) (2008) 7430–7437.
[8] D. Ohlund, E. Elyada, D. Tuveson, Fibroblast heterogeneity in the cancer wound, J. Exp. Med. 211 (8) (2014) 1503–1523.
[9] H.W. Jackson, V. Defamie, P. Waterhouse, R. Khokha, TIMPs: versatile extracellular regulators in cancer, Nat. Rev. Cancer 17 (1) (2017) 38–53.
[10] C. Ries, Cytokine functions of TIMP-1, Cellular and molecular life sciences, CMLS 71 (4) (2014) 659–672.
[11] G. Selvaraj, S. Kaliamurthi, S. Lin, K. Gu, D.Q. Wei, Prognostic impact of tissue inhibitor of metalloproteinase-1 in non-small cell lung cancer: systematic review and meta-analysis, Curr. Med. Chem. 26 (42) (2019) 7694–7713.
[12] B. Grünwald, B. Schoeps, A. Krüger, Recognizing the Molecular Multifunctionality and Interactome of TIMP-1, Trends Cell Biol. 29 (1) (2019) 6–19.
[13] J.D. Cohen, L. Li, Y. Wang, C. Thoburn, B. Afsari, L. Danilova, C. Douville, A.A. Javed, F. Wong, A. Mattox, R.H. Hruban, C.L. Wolfgang, M.G. Goggins, M. Dal Molin, T.-.L. Wang, R. Roden, A.P. Klein, J. Ptak, L. Dobbyn, J. Schaefer, N. Silliman, M. Popoli, J.T. Vogelstein, J.D. Browne, R.E. Schoen, R.E. Brand, J. Tie, P. Gibbs, H.-.L. Wong, A.S. Mansfield, J. Jen, S.M. Hanash, M. Falconi, P.J. Allen, S. Zhou, C. Bettegowda, L.A. Diaz Jr., C. Tomasetti, K.W. Kinzler, B. Vogelstein, A.M. Lennon, N. Papadopoulos, Detection and localization of surgically resectable cancers with a multi-analyte blood test, ScienceScience 359 (6378) (2018) 926.
[14] M.V. Rojiani, S. Ghoshal-Gupta, A. Kutiyanawalla, S. Mathur, A.M. Rojiani, TIMP-1 overexpression in lung carcinoma enhances tumor kinetics and angiogenesis in brain metastasis, J. Neuropathol. Exp. Neurol. 74 (4) (2015) 293–304.
[15] H. Cui, B. Seubert, E. Stahl, H. Dietz, U. Reuning, L. Moreno-Leon, M. Ilie, P. Hofman, H. Nagase, B. Mari, A. Krüger, Tissue inhibitor of metalloproteinases-1 induces a pro-tumourigenic increase of miR-210 in lung adenocarcinoma cells and their exosomes, OncogeneOncogene 34 (28) (2015) 3640–3650.
[16] S.-.A. Park, M.-.J. Kim, S.-.Y. Park, J.-.S. Kim, W. Lim, J.-.S. Nam, Y.Y. Sheen, TIMP-1 mediates TGF-beta-dependent crosstalk between hepatic stellate and cancer cells via FAK signaling, Sci. Rep. 5 (2015) 16492–16506.
[17] K.K. Jung, X.W. Liu, R. Chirco, R. Fridman, H.R. Kim, Identification of CD63 as a tissue inhibitor of metalloproteinase-1 interacting cell surface protein, EMBO J. 25 (17) (2006) 3934–3942.
[18] I.S. Aljada, N. Ramnath, K. Donohue, S. Harvey, J.J. Brooks, S.M. Wiseman, T. Khoury, G. Loewen, H.K. Slocum, T.M. Anderson, G. Bepler, D.F. Tan, Upregulation of the tissue inhibitor of metalloproteinase-1 protein is associated with progression of human non-small-cell lung cancer, J. Clin. Oncol. 22 (16) (2004) 3218–3229.
[19] J. Alcaraz, J.L. Carrasco, L. Millares, I.-.C. Luis, F.J. Fernández-Porras, A. Martínez-Romero, N. Díaz-Valdivia, J. Sánchez De Cos, R. Rami-Porta, L. Seijo, J. Ramírez, M.J. Pajares, N. Reguart, E. Barreiro, E. Monsó, Stromal markers of activated tumor associated fibroblasts predict poor survival and are associated with necrosis in non-small cell lung cancer, Lung Cancer 135 (2019) 151–160.
[20] L. Simi, M. Andreani, F. Davini, A. Janni, M. Pazzagli, M. Serio, C. Orlando, Simultaneous measurement of MMP9 and TIMP1 mRNA in human non small cell lung cancers by multiplex real time RT-PCR, Lung Cancer 45 (2) (2004) 171–179.
[21] S.A. Shah, F.G. Spinale, J.S. Ikonomidis, R.E. Stroud, E.I. Chang, C.E. Reed, Differential matrix metalloproteinase levels in adenocarcinoma and squamous cell carcinoma of the lung, J. Thorac. Cardiovasc. Surg. 139 (4) (2010) 984–990 discussion 990.

[22] Y. Hasegawa, S. Takanashi, Y. Kanehira, T. Tsushima, T. Imai, K. Okumura, Transforming growth factor-beta 1 level correlates with angiogenesis, tumor progression, and prognosis in patients with nonsmall cell lung carcinoma, Cancer-Cancer 91 (5) (2001) 964–971.
[23] R. Ikemori, M. Gabasa, P. Duch, M. Vizoso, P. Bragado, M. Arshakyan, I.C. Luis, A. Marin, S. Moran, M. Castro, G. Fuster, S. Gea-Sorli, T. Jauset, L. Soucek, L.M. Montuenga, M. Esteller, E. Monso, V.I. Peinado, P. Gascon, C. Fillat, F. Hilberg, N. Reguart, J. Alcaraz, Epigenetic SMAD3 repression in tumor-associated fibroblasts impairs fibrosis and response to the antifibrotic drug nintedanib in lung squamous cell carcinoma, Cancer Res. 80 (2) (2020) 276–290.
[24] M. Gabasa, R. Ikemori, F. Hilberg, N. Reguart, J. Alcaraz, Nintedanib selectively inhibits the activation and tumor-promoting effects of fibroblasts from lung adenocarcinoma patients, Br. J. Cancer 117 (2017) 1128–1138.
[25] C.M. Termini, J.M. Gillette, Tetraspanins function as regulators of cellular signaling, Front. Cell Dev. Biol. 5 (2017) 34.
[26] D. Forte, V. Salvestrini, G. Corradi, L. Rossi, L. Catani, R.M. Lemoli, M. Cavo, A. Curti, The tissue inhibitor of metalloproteinases-1 (TIMP-1) promotes survival and migration of acute myeloid leukemia cells through CD63/PI3K/Akt/p21 signaling, Oncotarget 8 (2) (2017) 2261–2274.
[27] R. Lugo, M. Gabasa, F. Andriani, F. Puig, F. Facchinetti, J. Ramírez, A. Gómez-Caro, U. Pastorino, G. Fuster, I. Almendros, P. Gascón, A. Davalos, N. Reguart, L. Roz, J. Alcaraz, Heterotypic paracrine signaling drives fibroblast senescence and tumor progression of large cell carcinoma of the lung, Oncotarget 7 (2016) 82324–82337.
[28] P. Bonniaud, M. Kolb, T. Galt, J. Robertson, C. Robbins, M. Stampfli, C. Lavery, P.J. Margetts, A.B. Roberts, J. Gauldie, Smad3 null mice develop airspace enlargement and are resistant to TGF-beta-mediated pulmonary fibrosis, J. Immunol. 173 (3) (2004) 2099–2108.
[29] M. Pesta, V. Kulda, R. Kucera, M. Pesek, J. Vrzalova, V. Liska, L. Pecen, V. Treska, J. Safranek, M. Prazakova, O. Vycital, J. Bruha, L. Holubec, O. Topolcan, Prognostic significance of TIMP-1 in non-small cell lung cancer, Anticancer Res. 31 (11) (2011) 4031–4038.
[30] R.L. Bigelow, B.J. Williams, J.L. Carroll, L.K. Daves, J.A. Cardelli, TIMP-1 overexpression promotes tumorigenesis of MDA-MB-231 breast cancer cells and alters expression of a subset of cancer promoting genes in vivo distinct from those observed in vitro, Breast Cancer Res. Treat. 117 (1) (2009) 31–44.
[31] J. Kobuch, H. Cui, B. Grünwald, P. Saftig, P.A. Knolle, A. Krüger, TIMP-1 signaling via CD63 triggers granulopoiesis and neutrophilia in mice, HaematologicaHaematologica 100 (8) (2015) 1005–1013.
[32] F. Aoudjit, S. Masure, G. Opdenakker, E.F. Potworowski, Y. St-Pierre, B. Gelatinase, MMP-9), but not its inhibitor (TIMP-1), dictates the growth rate of experimental thymic lymphoma, Int. J. Cancer 82 (5) (1999) 743–747.
[33] D.C. Martin, U. Rüther, O.H. Sanchez-Sweatman, F.W. Orr, R. Khokha, Inhibition of SV40 T antigen-induced hepatocellular carcinoma in TIMP-1 transgenic mice, OncogeneOncogene 13 (3) (1996) 569–576.
[34] M. Shimoda, S. Principe, H.W. Jackson, V. Luga, H. Fang, S.D. Molyneux, Y.W. Shao, A. Aiken, P.D. Waterhouse, C. Karamboulas, F.M. Hess, T. Ohtsuka, Y. Okada, L. Ailles, A. Ludwig, J.L. Wrana, T. Kislinger, R. Khokha, Loss of the Timp gene family is sufficient for the acquisition of the CAF-like cell state, Nat. Cell Biol. 16 (9) (2014) 889–901.
[35] P.D. Soloway, C.M. Alexander, Z. Werb, R. Jaenisch, Targeted mutagenesis of Timp-1 reveals that lung tumor invasion is influenced by Timp-1 genotype of the tumor but not by that of the host, OncogeneOncogene 13 (11) (1996) 2307–2314.
[36] S.J. Urbanski, D.R. Edwards, A. Maitland, K.J. Leco, A. Watson, A.E. Kossakowska, Expression of metalloproteinases and their inhibitors in primary pulmonary carcinomas, Br. J. Cancer 66 (6) (1992) 1188–1194.
[37] Z. Zhou, Q. Zhou, X. Wu, S. Xu, X. Hu, X. Tao, B. Li, J. Peng, D. Li, L. Shen, Y. Cao, L. Yang, VCAM-1 secreted from cancer-associated fibroblasts enhances the growth and invasion of lung cancer cells through AKT and MAPK signaling, Cancer Lett. 473 (2020) 62–73.
[38] S. Vicent, L.C. Sayles, D. Vaka, P. Khatri, O. Gevaert, R. Chen, Y. Zheng, A.K. Gillespie, N. Clarke, Y. Xu, J. Shrager, C.D. Hoang, S. Plevritis, A.J. Butte, E.A. Sweet-Cordero, Cross-species functional analysis of cancer-associated fibroblasts identifies a critical role for CLCF1 and IL-6 in non-small cell lung cancer in vivo, Cancer Res. 72 (22) (2012) 5744–5756.
[39] H. Li, Q. Zhang, Q. Wu, Y. Cui, H. Zhu, M. Fang, X. Zhou, Z. Sun, J. Yu, Interleukin-22 secreted by cancer-associated fibroblasts regulates the proliferation and metastasis of lung cancer cells via the PI3K-Akt-mTOR signaling pathway, Am. J. Transl. Res. 11 (7) (2019) 4077–4088.
[40] C. Lindskog, L. Fagerberg, B. Hallström, K. Edlund, B. Hellwig, J. Rahnenführer, C. Kampf, M. Uhlén, F. Pontén, P. Micke, The lung-specific proteome defined by integration of transcriptomics and antibody-based profiling, FASEB J. 28 (12) (2014) 5184–5196.
[41] M.S. Kwon, S.H. Shin, S.H. Yim, K.Y. Lee, H.M. Kang, T.M. Kim, Y.J. Chung, CD63 as a biomarker for predicting the clinical outcomes in adenocarcinoma of lung, Lung Cancer 57 (1) (2007) 46–53.
[42] M. Reck, R. Kaiser, A. Mellemgaard, J.-.Y. Douillard, S. Orlov, M. Krzakowski, J. von Pawel, M. Gottfried, I. Bondarenko, M. Liao, C.-.N. Gann, J. Barrueco, B. Gaschler-Markefski, S. Novello, L.U.-L.S. Grp, Docetaxel plus nintedanib versus docetaxel plus placebo in patients with previously treated non-small-cell lung cancer (LUME-Lung 1): a phase 3, double-blind, randomised controlled trial, Lancet Oncol. 15 (2) (2014) 143–155.
[43] L. Wollin, E. Wex, A. Pautsch, G. Schnapp, K.E. Hostettler, S. Stowasser, M. Kolb, Mode of action of nintedanib in the treatment of idiopathic pulmonary fibrosis, Eur. Respiratory J. 45 (5) (2015) 1434–1445.
[44] M. Zöller, Tetraspanins: push and pull in suppressing and promoting metastasis, Nat. Rev. Cancer 9 (1) (2009) 40–55.
[45] B. Seubert, H. Cui, N. Simonavicius, K. Honert, S. Schäfer, U. Reuning, M. Heikenwalder, B. Mari, A. Krüger, Tetraspanin CD63 acts as a pro-metastatic factor via β-catenin stabilization, Int. J. Cancer 136 (10) (2015) 2304–2315.
[46] L. Crombez, B. Marques, J.L. Lenormand, N. Mouz, B. Polack, C. Trocme, B. Toussaint, High level production of secreted proteins: example of the human tissue inhibitor of metalloproteinases 1, 337 (3) (2005) 908−915.
[47] J. Batra, J. Robinson, A.S. Soares, A.P. Fields, D.C. Radisky, E.S. Radisky, Matrix Metalloproteinase-10 (MMP-10) Interaction with Tissue Inhibitors of Metalloproteinases TIMP-1 and TIMP-2: BINDING, Studies and crystal structure 287 (19) (2012) 15935–15946.

[48] J. Domagała-Kulawik, G. Hoser, A. Safianowska, H. Grubek-Jaworska, R. Chazan, Elevated TGF-beta1 concentration in bronchoalveolar lavage fluid from patients with primary lung cancer, Arch. Immunol. Ther. Exp. (Warsz.) 54 (2) (2006) 143–147.
[49] L. Choy, J. Skillington, R. Derynck, Roles of autocrine TGF-beta receptor and Smad signaling in adipocyte differentiation, J. Cell Biol. 149 (3) (2000) 667–682.
[50] C. Salat-Canela, M. Sesé, C. Peula, S. Ramón y Cajal, T. Aasen, Internal translation of the connexin 43 transcript, Cell Commun. Signal 12 (2014) 31.
[51] K.J. Livak, T.D. Schmittgen, Analysis of relative gene expression data using real-time quantitative PCR and the 2 (-Delta Delta C(T)) Method, Methods 25 (4) (2001) 402–408.
[52] M. Abramoff, P. Magalhães, S.J. Ram, Image Processing with Image, J. Biophotonics Int. 11 (2003) 36–42.
[53] M. Gabasa, E.S. Radisky, R. Ikemori, G. Bertolini, M. Arshakyan, A. Hockla, P. Duch, O. Rondinone, A. Llorente, M. Maqueda, A. Davalos, E. Gavilán, A. Perera, J. Ramírez, P. Gascón, N. Reguart, L. Roz, D.C. Radisky, J. Alcaraz, MMP1 drives tumor progression in large cell carcinoma of the lung through fibroblast senescence, Cancer Lett. 507 (2021) 1–12.
[54] M. Uhlén, E. Björling, C. Agaton, C.A.-K. Szigyarto, B. Amini, E. Andersen, A.-C. Andersson, P. Angelidou, A. Asplund, C. Asplund, L. Berglund, K. Bergström, H. Brumer, D. Cerjan, M. Ekström, A. Elobeid, C. Eriksson, L. Fagerberg, R. Falk, J. Fall, M. Forsberg, M.G. Björklund, K. Gumbel, A. Halimi, I. Hallin, C. Hamsten, M. Hansson, M. Hedhammar, G. Hercules, C. Kampf, K. Larsson, M. Lindskog, W. Lodewyckx, J. Lund, J. Lundeberg, K. Magnusson, E. Malm, P. Nilsson, J. Ödling, P. Oksvold, I. Olsson, E. Öster, J. Ottosson, L. Paavilainen, A. Persson, R. Rimini, J. Rockberg, M. Runeson, Å. Sivertsson, A. Sköllermo, J. Steen, M. Stenvall, F. Sterky, S. Strömberg, M. Sundberg, H. Tegel, S. Tourle, E. Wahlund, A. Waldén, J. Wan, H. Wernérus, J. Westberg, K. Wester, U. Wrethagen, L. L. Xu, S. Hober, F. Pontén, A human protein atlas for normal and cancer tissues based on antibody proteomics, Molecular & Cellular Proteomics 4(12) (2005) 1920−1932.
[55] K. Kadota, J. Nitadori, K.M. Woo, C.S. Sima, D.J. Finley, V.W. Rusch, P.S. Adusumilli, W.D. Travis, Comprehensive pathological analyses in lung squamous cell carcinoma: single cell invasion, nuclear diameter, and tumor budding are independent prognostic factors for worse outcomes, J. Thorac. Oncol. 9 (8) (2014) 1126–1139.
[56] L. Grazioli, L. Olivetti, C. Fugazzola, A. Benetti, C. Stanga, E. Dettori, C. Gallo, L. Matricardi, A. Giacobbe, A. Chiesa, The pseudocapsule in hepatocellular carcinoma: correlation between dynamic MR imaging and pathology, Eur. Radiol. 9 (1) (1999) 62–67.
[57] M.E. Ritchie, B. Phipson, D. Wu, Y. Hu, C.W. Law, W. Shi, G.K. Smyth, limma powers differential expression analyses for RNA-sequencing and microarray studies, Nucleic Acids Res. 43 (7) (2015) e47-e47.
[58] Y.-F. Lee, C.-Y. Lee, L.-C. Lai, M.-H. Tsai, T.-P. Lu, E.Y. Chuang, CellExpress: a comprehensive microarray-based cancer cell line and clinical sample gene expression analysis online system, Database 2018 (2018).
[59] B. Győrffy, P. Surowiak, J. Budczies, A. Lánczky, Online survival analysis software to assess the prognostic value of biomarkers using transcriptomic data in non-small-cell lung cancer, PLoS ONE 8 (12) (2013) e82241.